Open Access

SCHÓLARENA

Journal of Nanoscience and Nanotechnology Applications

RESEARCH ARTICLE

ISSN: 2577-7920

# Linear and Nonlinear Optical Spectroscopy Characterization of MnTPYP-PMMA Composite Thin Films

**Sidiki Zongo[1, 2, *], Fabrice Bado[1], Tongonmanegde Léonard Ouedraogo[1], Moussa Sougoti[1], Sié Zacharie Kam[1], Téré Dabilgou[1], Benedo Josias Ouedraogo[1], Malik Maaza[1] and Antoine Béré[1]**

[1]*Laboratoire de Physique et de Chimie l'Environnement (LPCE) Université Joseph KI-ZERBO, 03 PO. Box 7021 Ouagadougou 03-Burkina Faso*

[2]*UNESCO-UNISA Africa Chair in Nanosciences/Nanotechnology, University of South Africa, Muckleneuk Bridge, PO. Box 392, Pretoria-South Africa*

[*]**Corresponding Author:** Sidiki Zongo, Laboratoire de Physique et *de Chimie* l'Environnement (LPCE) Université Joseph KI-ZERBO, 03 PO. Box 7021 Ouagadougou 03- Burkina Faso, E-mail: sidiki.zongo@yahoo.fr

**Citation:** Sidiki Zongo, Fabrice Bado, Tongonmanegde Léonard Ouedraogo, Moussa Sougoti, Sié Zacharie Kam et al. (2024) Linear and Nonlinear Optical Spectroscopy Characterization of Mntpyp-PMMA Composite Thin Films, J Nanosci Nanotechnol Appl 8: 104

**Received Date:** October 24, 2024 **Accepted Date:** November 24, 2024 **Published Date:** December 01, 2024

## Abstract

The substantial-good electron π-conjugation observed in all-metalloorganic complexes and porphyrin derivatives are suitable as potential third-order nonlinear optical (NLO) materials application. The central metal ion configuration renders these complexes more advantageous in the nonlinear optical response induced by charge displacement and the effect of the external field compared to many other organic and inorganic materials. This paper, we assess the linear optical and nonlinear optical properties of tetra-porphine magnesium (MnTPyP)-polymethyl methacrylate (PMMA) composite thin films prepared by a simple coating technique. Based on the Drude model single oscillator calculations, other optical parameters such as dispersion energy, dielectric constant nonlinear refractive index and the third nonlinear susceptibility were evaluated and addressed in detail.

**Keywords:** Inorganic Materials; Tetra-Porphine Magnesium; Optical Spectrophotometric; Dispersion Energy; Dielectric Constant; Nonlinear Susceptibility; Single Oscillator

## Introduction

Much of the reports dealing with electro-optical and nonlinear–optical technologies highlight the significant role of organic and inorganic materials. Thus, multi-functional metal-organic materials, including metalloporphyrin complexes and derivatives have attracted much attention over the years [1, 2] in several research groups. As a great deal of concerted efforts, organometallic complexes have brought to light a substantial understanding of the structure-function relationship in these complex compounds [3, 4] and their applications. These compounds present numerous advantages, consisting of a combination of propensities for individual components such as inorganic metal ions and organic ligands. Generally, the polar character of metal–to–ligand bonds usually are characterized by a large transition moment as well as a large excited state dipole moment, allowing enhanced hyperpolarizability (b) and in parallel second-order nonlinear optical susceptibility [5, 6]. Also, these molecular templates allow: (i) Structural functionalization of the molecular scaffold of the organic ligands, thus tuning easy their optical and NLO properties along with the coordination ability to the metal ion; (ii) Isolation of mixed–metallic and polynuclear compounds determining chemical-physical effects on the base on properties of the metal–centres along with those associated with the ligands, as mentioned in (i); (iii) Isolation of diversity of self–assembly structures of crystals of metal–organics; (iv) High optical and NLO efficiency; (v) Good–to–excellent crystal growth; (vi) High thermal stability without melting point processes. Due to their specific spatial and electronic structures, synthetic porphyrins and metalloporphyrin have inspiring biological, photophysical and photochemical properties and have been revealed to be potential candidates for disease treatment as reported by Ptaszyńska et al., 2018 [7]. Biological imaging through tomography biodistribution studies was conducted by Varchi et al., 2015 [8] and Cheng et al., 20214 [9]. Interest in metalloporphyrins is not confined only to the biological field [10, 11] but plays a crucial role from technological and industrial points of view. During the last two decades, synthetic porphyrins were investigated for various applications other than chemical and electrochemical. Porphyrins and metalloporphyrin were proven to be radio-diagnostic agents in photodynamic therapy, semiconductors, and photovoltaic materials [12, 13], for which applications several patents have been lodged. Zucca et al., 2016 [14] have focused their investigation on the industrial application. They found a tremendous utilization of synthetic formulations of metalloporphyrin compounds in textiles. The catalytic effect of metalloporphyrins as electroactive agents in ion-selective membranes was reported to be a unique reagent in spectrophotometry [15]. The organometallic framework carried out in the group of Leng et al., 2018 [16] has demonstrated a potential for catalysis, particularly in the structural-property relationships. In addition to the abovementioned applications, NLO properties of metalloporphyrins are widely investigated 17, 18]. In their review, Dini et al., 2016 [19] emphasized the photoactive materials for optical power limiting. Few investigations involving nonlinear properties of magnesium porphyrins have been reported [20]. These studies concern the nonlinear and transient absorption spectroscopy of magnesium (II)-tetra-benzoporphyrin (Mg-TBP) in solution. In the present work, we investigate the optical and nonlinear optical properties of tetra-porphine manganese (MnTPyP)-polymethyl methacrylate (PMMA) composite thin films.

### Experimental Procedure

### Material and Thin Film Preparation

Mg 5,10,15,20-tetra(4-pyridyl)-21H,23H-Prophine Dye content 90% (MnTPyP) and PMMA polymer were purchased from Aldrich Chem. Co. and used as received without any further purification. The schematic diagram of the MnTPyP molecular structure is shown in Figure 1**.** Thin films of MnTPyP doped PPMA were prepared onto well-cleaned optically flat fused glass substrates by the spin coating technique at different rpm using EDC-650-23 coating unit. Tree different average thicknesses of 50 nm, 160 nm and 260 nm thin films were prepared at coating speed of 800, 1600 and 4000 rpm respectively at room temperature. The films were dried and kept at ambient temperature for further use.

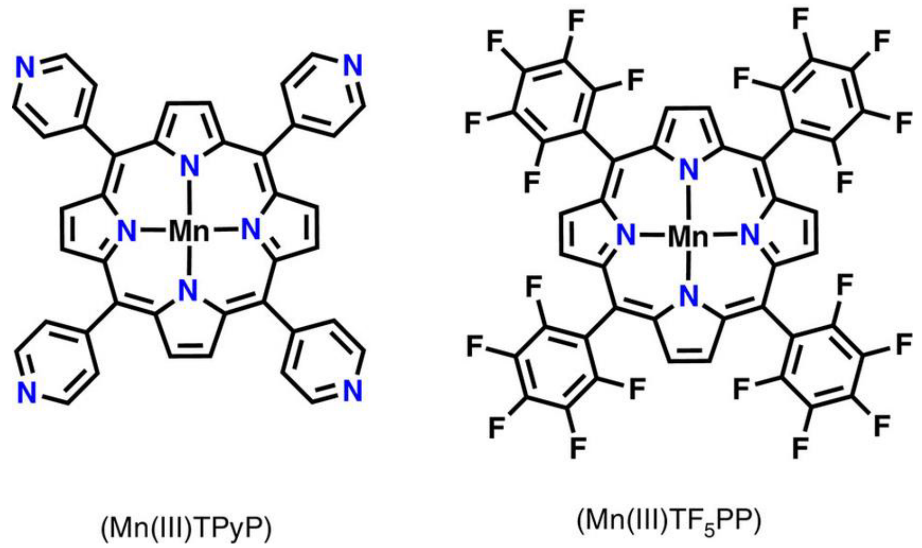


**Figure 1:** MnTPyP molecular structure

## Optical Measurements

The reflectance R(k) and transmittance T(k) spectra of the MgTPyP-PMMA thin films were recorded at normal incidence of light in the spectral range 200–2500 nm using a double beam spectrophotometer (JASCO model V-730 UV–VIS–NIR). The obtained spectral data from the spectrophotometer were converted to absolute values to eliminate the reflectance and absorbance of the substrate. The absolute values of T and R are given by the governing equations in [21]:

$$T = \left(\frac{I_{lt}}{I_{lr}}\right)(1 - R_{lr}) \quad (1)$$

$$R = \left(\frac{I_{lr}}{I_{lm}}\right) R_m \left(1 + [1 - R_{lr}]^2\right) - T^2 R_{lr} \quad (2)$$

Where $I_{lt}$ is the intensity of the light passing through film-quartz structure, $I_{lr}$ is the intensity of reflectance from quartz substrate and $R_{lr}$ is the quartz reflectance. $I_{lr}$ and $I_m$ are the light intensities reflected from the composite film and from the reference mirror, respectively and $R_m$ is the reflectance of the reference mirror. According to a program developed by El-Nahass et al., 2015 [21] the extinction coefficient k, the absorption coefficient α and the refractive index n were calculated through the following equations reported in [22].

$$\alpha = \frac{1}{t}\left[\frac{(1-R)^2}{2T} + \sqrt{\frac{(1-R)^4}{4T^2} + R^2}\right] \quad (3)$$

$$k = \frac{\alpha\lambda}{4\pi} \quad (4)$$

$$n = \left(\frac{1+R}{1-R}\right) + \sqrt{\frac{4R}{(1-R)^2} - R^2} \quad (5)$$

## Results and Discussion

### Linear Optical Characterization of MnTPyP-PMMA Composite Thin Films

### FTI-R Spectra

FTIR is an analytical technique based on vibration and absorption of the interatomic bonds in organic/inorganic compounds. It is mainly utilized in the determination of the structure of organic compounds. As a strong bond type dependent, each bond in the organic material absorbed a specific frequency at varying intensity. Thus, IR spectra result from absorption information and analysis of the organic material [23]. FTIR spectra in the range 400–1500 $cm^{-1}$ of both powder and as-deposited MnTPyP-PMMA composite thin films are illustrated in Figure 2 a & b. Table 1 depicts the revealed IR bands and their assignments. The band at 621 and 1338 corresponds to the phenyl aromatic compound. The band appearing at 1008 $cm^{-1}$ is assignable to the Cb-H rocking vibration of the pyrrole ring [24], entirely describes the metallated porphyrin. The FTIR spectrum of the composite thin film does not vary significantly with evaporation and the added PPMA material, demonstrating that the deposition process is a good one to obtain undissociated and stoichiometric MnTPyP-PMMA films. Moreover, the FTIR spectrum of the thin film is very similar to that of the powder.

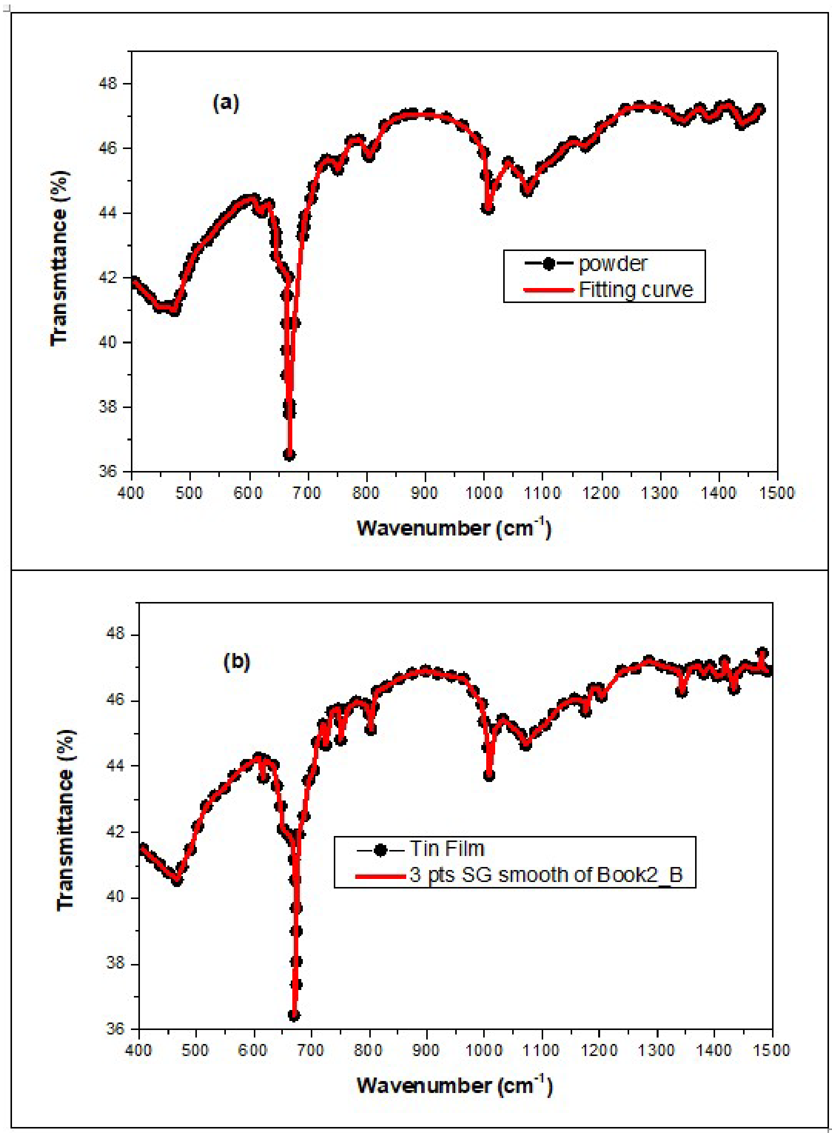


**Figure 2:** (a) Infrared spectra of MnTPyP-PMMA for the powder (b) as-deposited film.

**Table 1:** The position of band in IR spectra of different forms of MnTPyP-PMMA

| Wavenumber ($cm^{-1}$) | | Assignment |
|---|---|---|
| Powder | Thin film | |
| 621 | 619 | Phenyl |
| 670 | 669 | γ(Cb-H)sym. |
| 720 | 720 | δ(pyr. deform.)sym |
| 755 | 753 | δ(pyr. deform.)sym |
| 807 | 802 | δ(pyr. deform.)sym |
| 1008 | 1008 | δ (Cb-H)asym. |
| 1078 | 1073 | δ (Cb-H)asym. |
| 1173 | 1176 | δ (Cb-H)asym. |
| 1201 | 1204 | δ (Cb-H)asym |
| 1338 | 1347 | Phenyl |
| 1386 | --- | --- |

## Transmittance and Reflectance Spectra

Figure 3 presents the optical reflectance and transmittance of MnTPyP-PMMA composite thin films measured at normal incidence in the wavelength ranging from 200 to 2500 nm. At wavelengths below 400 nm, the material absorbs. In the UV-visible region (i.e. 400 nm, sharp band edge absorptions, where the peak position is independent of the thickness are observed for all samples. The appearance of such bands indicated that the studied material is promising for optical filter application. At longer wavelengths above 700 nm, the spectral distribution shows that all three samples are transparent to the incident light. No significant light absorption or scattering is observed.

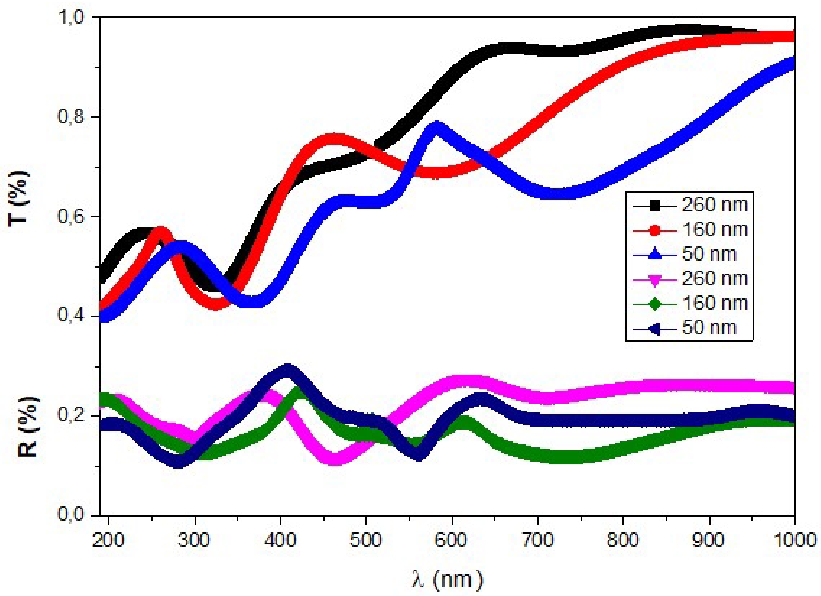


**Figure 3:** The spectral dependence of the transmittance T (%) and reflectance, R %k) of the as-deposited MnTPyP-PMMA composite thin film at different thickness, respectively.

## Dispersion and Refractive Index Evaluation

The spectral distribution of the refractive index *(n)* and the extinction coefficient *(k)* of prepared material in Figure 4 a & b are plotted from the mean values and k, independent on the films thickness. At $\lambda<700$ *nm*, the spectra present a dispersion with multiple peaks for which an appropriate multiple oscillator model [25] can be used. The observed dispersion is associated to the resonance effect resulted from incident light and the electron's polarization. In the transparent region (i.e. $\lambda > 700$ *nm*), the normal dispersion observed can be model through a single oscillator [23] and the extracted portion is presented in Figure 5a. The refractive index is approximated to be 2.158, 2.297 and 2,367 at $\lambda > 800$ nm for 50 nm, 160 nm and 260 nm respectively. The dependency between the high- frequency dielectric constant

$(\varepsilon_L)$ involving refractive index *(n)* and wavelength were estimated through the relation

$$n^2 = \varepsilon_L - \left(\frac{e^2}{4\pi^2 c^2 \varepsilon_0}\right)\left(\frac{N}{m^*}\right)\lambda^2 \quad (6)$$

where 'e' corresponds to the electronic charge, ε0 is the permittivity of free space, and N/m* is the ratio between the effective masses and no. of charge carriers. The parameters εL and N/m* were calculated from the vertical intercept and slope of the $n^2$ vs. $\lambda^2$ presented in Figure 5b.

As a significant tool in appreciating various photonic and spectral dispersion devices, the dispersion energy $(E_d)$ and oscillator energy $(E_0)$ were evaluated from a single effective oscillator model introduced by Wemple & Di-Domenico (WDD) **[25]** using the following equation.

$$\frac{1}{n^2-1} = \frac{{E_0}^2-(h\vartheta)^2}{E_0 E_d} = \frac{E_0}{E_d} - \frac{(h\vartheta)^2}{E_0 E_d} \quad (7)$$

where $E_o$ is the oscillator energy for electronic transitions and Ed is the dispersion energy. Both $E_d$ and $E_0$ are determined from slope $(E_0\, E_d)^{-1}$ and intercept $\left(\frac{E_0}{E_d}\right)$ values of $(n^2-1)^{-1}$ *vs.* $(h\vartheta)^2$ plot in Figure 4d. The value of $E_d$ represents the average strength of interband transition while $E_0$ approximates the separation between the centres of gravity of the valence and conduction band. It can be observed that both parameters decrease with film thickness. The oscillator strength of the material defined by $f=E_0.E_d$ calculated is also indicated in Table 1. In this figure, the extrapolating of straight lines to the points of interception at $(h\vartheta)^2 = 0$ gives the value of $n_\infty^2 = \varepsilon_\infty = n_0^2$ which is computed and given in Table 2.

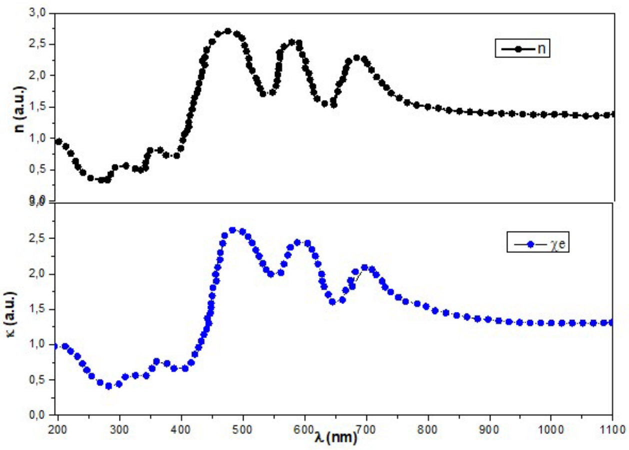


**Figure 4:** spectral distribution of the refractive index *(n)* in panel *(a)* and the extinction coefficient *(k)* in panel *(b)* of prepared material.

**Table 2:** Dispersion and non-linear optical parameters of the as-deposited MnTPyP-PMMA composite thin films

| *d (nm)* | *$E_0$(eV)* | *$E_d$(eV)* | *$E_0E_d(eV)^2$* | *$n_0$* | *$\varepsilon_\infty$* | *$\lambda_0$ (nm)* | *$S_0 \cdot 10^{12}$ ($m^{-2}$)* | *$\chi^{(1)}$ (esu.)* | *$\chi^{(1)}$ $10^{-14}$ (esu.)* | *$n_2^* 10^{-2}$(esu.)* |
|---|---|---|---|---|---|---|---|---|---|---|
| 50 | 2.252 | 2.719 | 6.123 | 1.486 | 2.208 | 355.45 | 9.56 | 0.096 | 1.4439 | 0.3678 |
| 160 | 2.494 | 4.356 | 10.864 | 1.687 | 2.846 | 355.45 | 14.611 | 0.147 | 7.9381 | 2.022 |
| 260 | 3.03 | 7.786 | 23.59 | 1.889 | 3.568 | 355.45 | 20.323 | 0.204 | 29.445 | 7.499 |

In the transparent (non-absorbing) region, the average inter-band oscillator wavelength $\lambda_0$ and the average oscillator strength S of the as-prepared MnTPyP-PMMA composite thin film. From sellmeier single term dispersion relation [26], n is associated to the wavelength as following [27]:

$$\frac{(n_0^2-1)}{(n^2)} = 1 - \left(\frac{\lambda_0}{\lambda}\right)^2 \quad (8)$$

Where k is the incident photon wavelength $\lambda_0$ and no is the refractive index at zero frequency (static refractive index). The values $n_0$ and $\lambda_0$ were calculated from the Plotting of $(n^2\text{-}1)^{-1}$ against $(\lambda^2)^{-1}$ as shown in Fig. 4d. Rearranging of Equation (8) led [27]:

$$n^2 - 1 = \frac{(S_0\lambda_0)}{(1-\lambda_0^2/\lambda^2)} \quad where \quad S_0 = (n_0^2-1)/\lambda_0^2 \quad (9)$$

From this table, we observed that the optical and nonlinear optical parameters increased as the thickness of the film increasing. This observation is made with the tetratolylporphine manganese (III) chloride (MnTTPCl) [28].

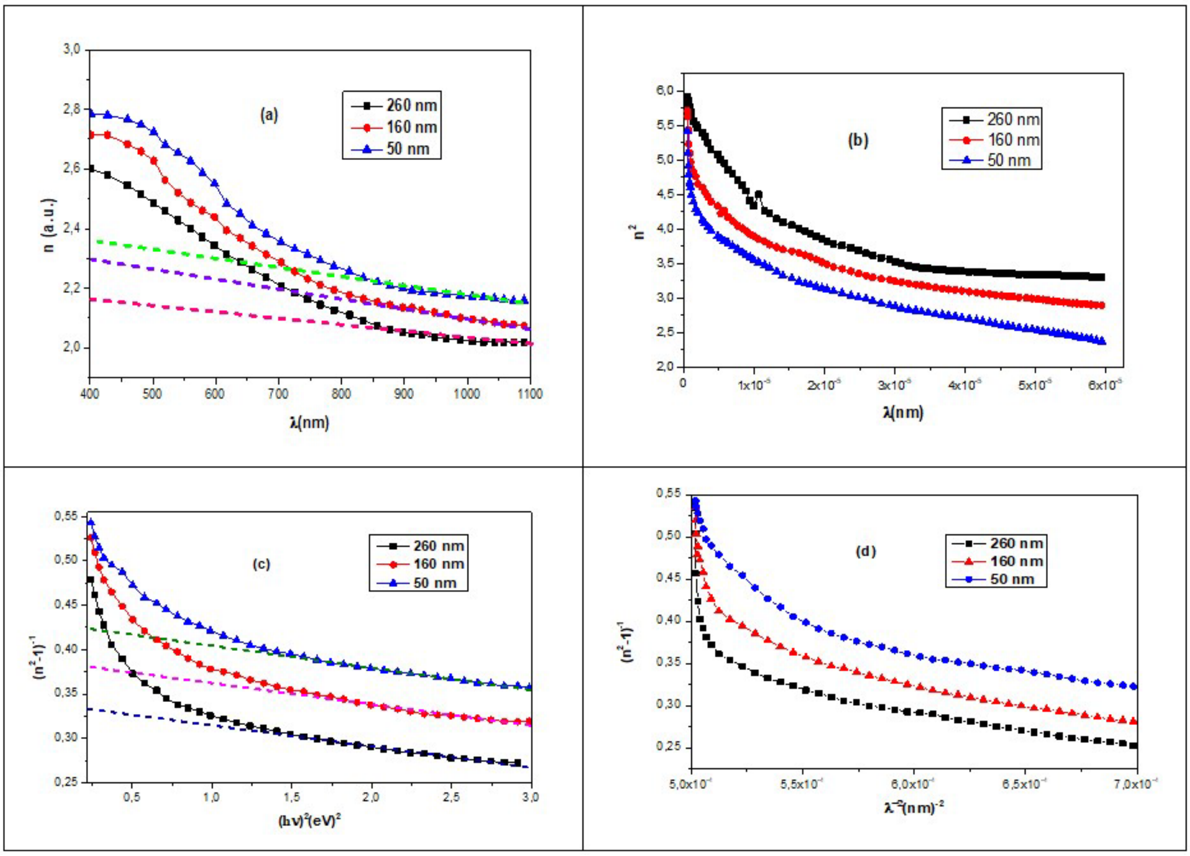


**Figure 5:** (a) *'n' vs. 'λ'; (b) $n^2$ vs. $\lambda^2$; (c) $(n^2\text{-}1)^{-1}$ vs. $(h\vartheta)^2$* and *(d) $(n^2\text{-}1)^{-1}$* against *$(\lambda^2)^{-1}$*; all at different thicknesses.

## Nonlinear Optical Properties

When a material is exposed to high light intensity, the polarization is no longer linearly proportional to the incident electric field *E*. Therefore, a nonlinear phenomenon is produced through the medium. Nonlinear optical properties of material play an important role in nonlinear optical devices such as all-optical switching, optical power limiting, image manipulation and image processing, integrated photonic devices, etc. The nonlinear relation between optical parameters and electric field in chalcogenide materials refers to optical nonlinearity. The source of the optical nonlinearity arises due to the nuclear interactions with electronic polarizability and hence influences bond lengths. This phenomenon arises owing to the net polarization developed in materials upon intense exposure to the light beam. The net dipole moment is directly proportional to the susceptibility $(P= \varepsilon_0, \chi, E)$, where it stands for the permeability of free space, and $E$ stands for the electric field intensity. where $\varepsilon_0$ stands as permeability of free space and E, the electric field intensity. The polarization P can be expressed following equation [29].

$$P = \chi^{(1)}E + \chi^{(2)}E + \chi^{(3)}E + \ldots \quad (10)$$

Where $\chi^{(i)}$ refers to the linear optical susceptibility, $\chi^{(i)}$ $(i\geq 2$ is ith the order nonlinear susceptibility. The value of $\chi^{(i)}$ is often calculated using the single oscillator parameters Eo; Ed and the photon energy [22, 30]. For isotropic medium, $\chi^{(i)}$ can be expressed as function of the linear refractive, given relation [22, 30-32].

$$\chi^{(1)} = \left[\frac{E_0 E_d}{4\pi\left({E_0}^2 - (h\vartheta)^2\right)}\right] = \frac{n^2-1}{4\pi} \quad (11)$$

Third-order nonlinear optical susceptibility $\chi^{(3)}$ variation is determined through a combination of Miller's principles and the Wemple single oscillator model and is calculated from the equation.

$$\chi^{(3)} = A\left[\frac{n_0^2-1}{4\pi}\right]^4 \quad (12)$$

Where $n_0$ is the static refractive index, $A=1.7\ 10^{-10}$ (e.s.u) in the limit $h\vartheta \to 0$ $(n = n_0)$ is a constant for all nonlinear material and is assumed to be frequency independent. The nonlinear refractive index is evaluated through a combination of Miller's principles and static refractive index $n_0$ and given by [29, 33].

$$n_2 = \frac{12\pi}{n_0}\chi^{(3)} \quad (13)$$

Table 1 displays the computed $\chi^{(1)}$ , $\chi^{(3)}$ and $n_2$. All the parameters increase with the thickness. In this investigation, we observed a change in the refractive index with the thickness of the films. In certain materials, the refractive index change of the sample is detected by monitoring the change in the output transmission. In such detection schemes, employing low-loss dielectric optical micro-resonators can significantly improve the device's sensitivity. Moreover, the long photon lifetime for an optical signal travelling inside these resonators is responsible of a strong interaction between the surrounding materials and the optical modes, which makes the optical resonance frequency susceptible to perturbations.

The nonlinearity results from the increase in the nonlinear refractive index, as demonstrated by Shanmugavelu et al., 2013 [34]. This improvement may also result from the thickness due to the quantum size effects. This analysis shows that as-prepared materials are good candidates for all-optical switching applications, image processing, and suitable for various photonic applications like, high-speed communication devices, optical limiter, because molecules with high $\chi^{(3)}$ have high loss due to two-photon absorption [34].

## Dielectric Constant& Loss Factor

The dielectric and optical properties of the material are essential in defining the polarizability of the material. Thus, the complex dielectric function which defines the reflection, the propagation and the optical loss in the material is vital for various opto-electronic and photonic applications. The governing complex dielectric function is given by the relation [35].

$$\varepsilon^* = \varepsilon_r + i\varepsilon_i = (n + ik)^2 \quad (14)$$

where $\varepsilon_r$ and $\varepsilon_i$ are the real and imaginary part of the dielectric constant and satisfying the following relations,

$$\varepsilon_r = n^2 - k^2 \quad and \quad \varepsilon_i = 2nk \quad (15)$$

where *n* and *k* correspond to the linear refractive index and extinction coefficient of thin films.

The real part ($\varepsilon_r$) characterizes the dispersion of light interacting within the material. It is also responsible for the decrease in the propagation speed. The imaginary part ($\varepsilon_i$) refers to the energy absorbed from the associated electric field due to the dipolar movement. Figures 6a & b present the corresponding behaviour of $\varepsilon_r$ and $\varepsilon_i$ of the dielectric constant vs. the wavelength. These behaviours suggest a decrease in the energy dissipated and an increase in the perturbation rate of the electromagnetic wave, as indicated by [36]. Since $\varepsilon_r$ and $\varepsilon_i$ act as mirrors of the material characteristics, it is necessary to study these parameters, which are essential to the design of photonics and optoelectronic devices. From εr and εi, the dissipation factor or dielectric loss of material can be described by the relation *tan(δ)*= $\varepsilon_r/\varepsilon_i$ [37] where *δ* is the loss angle. This parameter defines the phase difference of loss energy at the considered frequency of the material. Figure 7 depicts the plot of this loss factor of as-prepared MnTPyP-P-MMA thin films versus the photon energy. The corresponding behaviour results from the incapability of molecules to reorient themselves with the incident electric field.

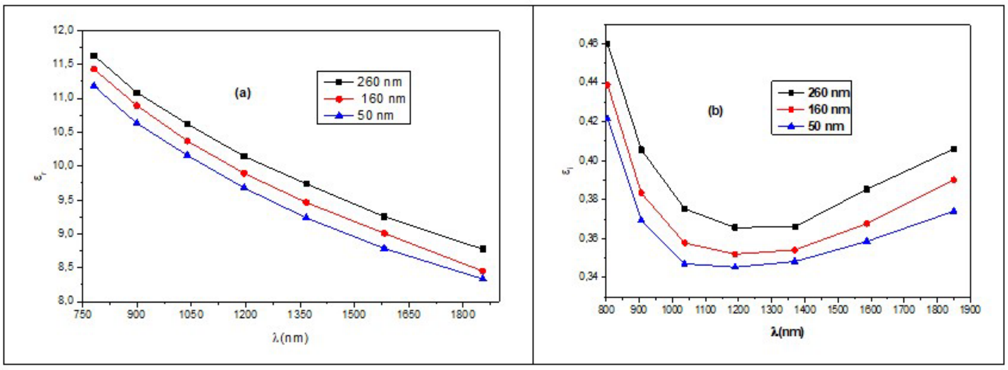


**Figure 6:** (a) $\varepsilon_r$ *vs. λ* for the film at different thickness (b) $\varepsilon_i$ *vs. λ* for the film at different thickness.

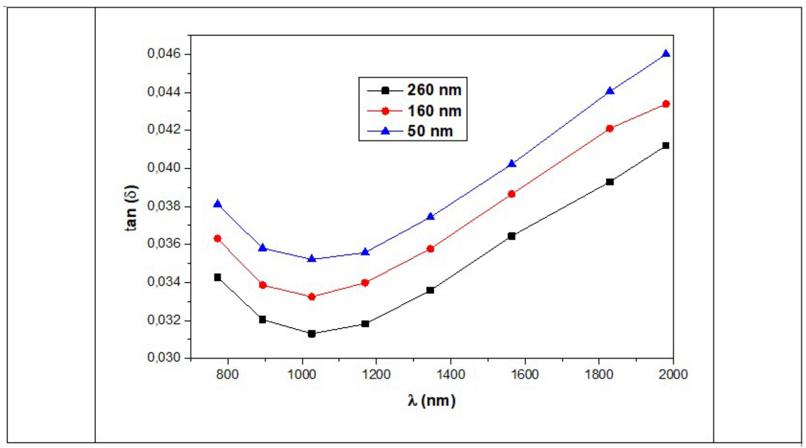


**Figure 7:** Dielectric loss factor at different thickness.

**Optical Conductivity ($\sigma_{opt}$) and Electrical Conductivity ($\sigma_{elec}$)**

Optical conductivity represents the frequency response of the material exposed to the optical excitation. Moreover, in association with the electrical conductivity gives the information related to the electronic state of the material. These two parameters which depend upon *λ*, *n*, *α* and *c* are described by the useful equations as follow:

$$\sigma_{opt} = \frac{\alpha n c}{4\pi} \quad and \quad \sigma_{elec} = \frac{2\lambda\sigma_{opt}}{\alpha}$$

where c the velocity of light.

The variation these two optical and electrical conductance ($\sigma_{opt}$ & $\sigma_{elc}$) parameters are of as deposited thin film shown in Figure 8a & b. The values of $\sigma_{opt}$ increase with the film thickness. The increase in the optical conductance results from the increase in absorption coefficient with $hv$, owing to the electronic excitation across the band due to the photon energy. The decreasing behaviour is observed with $\sigma_{elc}$ inversely proportional to *α*.

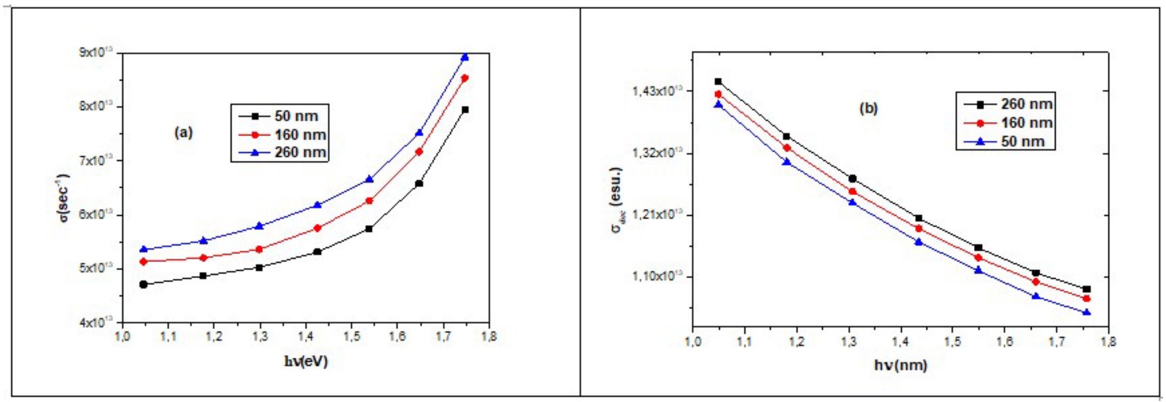


**Figure 8:** Variation of (a) $\sigma_{opt}$ (b) $\sigma_{elc}$ at different thin film thickness of as-prepared.

The porphyrin-based donor-acceptor (D-A) systems have been explored over the years for their tunable optical and electronic properties to improve the efficacy of many applications, including organic light emitting diodes, photodynamic therapy, nonlinear optics, dye-sensitized solar cells, single molecule switches, photodetectors, window layers, sensors and many more. The possibility of tailoring the optical and electrical parameter values is a proper addition to the nano-fabric thin films of high-conductivity nanoparticles for enhancing the electrical conductivity by orders of magnitude but by applying an external magnetic or electric field.

## Conclusion

The MnTPyP-PMMA composite thin films at different thickness were prepared. The linear optical properties were recorded through spectrophotometric measurements. It was found that the refractive index dispersion in the transparent region (i.e. *λ>700 nm*) obey the single oscillation model developed by Wempl Di-Domenico (WDD) single effective oscillator model and the approximated refractive index was about 2.158, 2.297 and 2,367 at for 50 nm, 160 nm and 260 nm. The change in the dispersion behaviour prove the potential of developing high performant photonics and optoelectronic devices. The investigation of optical conductivity revealed a hight values which confirm the presence of induced hight photo response of the material whereas, lower electrical conductivity values indicate the semiconducting character of the material. The nonlinear refractive index $n_2$ and the non-linear optical susceptibility $\chi^{(3)}$ obtained fascinating for the manufacture of nonlinear optical devices.

## Conflicts of Interest

There are no conflicts to declare

## Acknowledgements

The present work was partially supported the UJKZ-SEA 2024TG-and the Optical Platform at iThemba LABS in South Africa

## References

1. M Pineiro, AL Carvalho, MM Pereira, AM d'AR Gonsalves, LG Arnaut et al. (1998) Photoacoustic Measurements of Porphyrin Triplet-State Quantum Yields and Singlet-Oxygen Efficiencies ", Chem. Eur. J, 4: 2299-307.

2. S Lesage, H Xu, L Durham (1993) The occurrence and roles of porphyrins in the environment: possible implications for bioremediation ", hydrological sciences bulletin des sciences hydrologiques, 38: 343-54.

3. Long NJ (1995) Organometallic Compounds for Nonlinear Optics-The Search for En-light-enment. Angew. Chem. Int. Ed. Engl, 34: 21–38.

4. Ian R Whittall, Mark G Humphrey, Stephan Houbrechts, Joachim Maes, André Persoons et al. (1997) Organometallic complexes for nonlinear optics. 14. Syntheses and second-order nonlinear optical properties of ruthenium, nickel and gold σ-acetylides of 1,3,5-triethynylbenzene: Journal of Organometallic Chemistry, 544: 277-83.

5. Francesca Tessore, Alessio Orbelli Biroli, Gabriele Di Carlo, Maddalena Pizzotti (2018) Porphyrins for Second Order Nonlinear Optics (NLO): An Intriguing History. Inorganics, 6: 81.

6. Cui-Cui Yang, Li Li, Wei Quan Tian, Wei-Qi Li, Ling Yang (2022) Strong second order nonlinear optical properties of azulene-based porphyrin derivatives. Phys Chem Chem Phys, 24: 13275-85.

7. Aneta A Ptaszyńska, Mariusz Trytek, Grzegorz Borsuk, Katarzyna Buczek, Katarzyna Rybicka-Jasińska et al. (2018) Porphyrins inactivate Nosema spp. microsporidia. Sci. Rep, 8: 5523.

8. Greta Varchi, Federica Foglietta, Roberto Canaparo, Marco Ballestri, Francesca Arena et al. (2018) Engineered porphyrin loaded core-shell nanoparticles for selective sonodynamic anticancer treatment. Nanomedicine. Nanomedicine (Lond), 10: 3483-94.

9. Weiran Cheng, Inga E Haedicke, Joris Nofiele, Francisco Martinez, Kiran Beera et al. (2021) Complementary Strategies for Developing Gd-Free High-Field T 1 MRI Contrast Agents Based on MnIII Porphyrins. J. Med. Chem, 57: 516-20.

10. Fabien Hammerer, Guillaume Garcia, Su Chen, Florent Poyer, Sylvain Achelle et al. (2014) Synthesis and characterization of glycoconjugated porphyrin triphenylamine hybrids for targeted two-photon photodynamic therapy. J. Organ. Chem, 79: 1406–17.

11. Xia Dong, Hongli Chen, Jingwen Qin, Chang Wei et al. (2017) Thermosensitive porphyrin-incorporated hydrogel with four-arm PEG-PCL copolymer(II): Doxorubicin loaded hydrogel as a dual fluorescent drug delivery system for simultaneous imaging tracking in vivo. Drug Deliv, 24: 641-50.

12. Juan C Barona-Castaño, Christian C Carmona-Vargas, Timothy J Brocksom, Kleber T de Oliveira (2016) Porphyrins as Catalysts in Scalable Organic Reactions., Molecules, 21: 310.

13. I Ievgen Obraztsov, Wlodzimierz Kutner, Francis D'Souza et al. (2017) Evolution of Molecular Design of Porphyrin Chromophores for Photovoltaic Materials of Superior Light-to-Electricity Conversion Efficiency, Sol. RRL, 1600002.

14. Paolo Zucca, Cláudia M B Neves, Mário M Q Simões, Maria da Graça P M S Neves et al. (2017) Immobilized lignin peroxidase-like metalloporphyrins as reusable catalysts in oxidative bleaching of industrial dyes. Molecules, 21: 964.

15. Ramesh Chandra, Manisha Tiwari, Parvinder Kaur, Meenakshi Sharma, Ritu Jain et al. (2000) Metalloporphyrins - Applications and Clinical Significance. Indian Journal of Clinical Biochemistry, 15: 183-99.

16. Ruolan Li, Zongqian Wu, Ya Chen, Xingyan Liu, Weiwei Guo et al. (2018) Boosting Photocatalytic Hydrogen Production of Porphyrinic MOFs: The Metal Location in Metalloporphyrin Matters. ACS Catal, 8: 4583-90.

17. Xuewei Huang, Fengli Wei, Fengqi Guo, Yanyan Zhu (2020) Synthesis, crystal structure and nonlinear optical properties of ferrocene-containing metalloporphyrins. Inorganica Chimica Acta, 511: 119816.

18. Qian Zhang, Bishuai Lu, Shan Liu, Xiangfei Lü, Xuemei Cheng (2023) Mechanism of optical limiting in metalloporphyrins under visible continuous radiation. Physical Chemistry Chemical Physics. 41: 2023.

19. S Dini, BJ Binder, SC Fische JR (2023) Identifying the necrotic zone boundary in tumour spheroids with pair-correlation functions Soc. Interface, 13: 20160649.

20. H Stiel, A Volkmer, I Rückmann, A Zeug, B Ehrenberg, B Röder (2022) Non-linear and transient absorption spectroscopy of magnesium(II)-tetrabenzoporphyrin in solution. 21. MM El-Nahass, H Kamal, MH Elshorbagy, K Abdel-Hady (2013) Structural and optical properties of chromotrope 2R thin films of different thicknesses, OptikInt. J. Light Electron Opt, 124: 6718-626.
22. HM Zeyada, MM Makhlouf, MM El-Nahass (2015) Influence of gamma ray irradiation and annealing temperature on the optical constants and spectral dispersion parameters of metal-free and zinc tetraphenylporphyrin thin films: a comparative study, Spectrochim. Acta Part A: Mol. Biomol. Spectrosc, 148: 338-47.

21. MM El-Nahass, HM Zeyada, KF Abd-El-Rahman, AAM Farag, AAA Darwish, Spectrochim et al. (2008) Acta Part A Mol. Biomol. Spectrosc, 69: 205.

22. J Vongsvivut, T Itoh, A Ikehata, S Ekgasit, Y Ozaki (2006) Surface-Enhanced Infrared Spectra of Manganese (III) Tetraphenylporphine Chloride Physisorbed on Gold Island Films Sci. Asia, 32: 261.

23. SH Wemple (1973) Refractive-index behavior of amorphous semiconductors and glasses, Phys. Rev. B, 7: 3767.

24. M Dongol, MM El-Nahass, A El-Denglawey, AF Elhady, AA Abuelwafa (2012) Optical properties of nano 5, 10, 15, 20-tetraphenyl-21H, 23H-prophyrin nickel (II) thin films, Curr. Appl. Phys. 12: 1178–84.

25. F Yakuphanoglu, A Cukurovali, I Yilmaz (2004) Determination and analysis of the dispersive optical constants of some organic thin films, Phys. B: Condens. Matter, 351: 53–8.

26. SR Alharbi, AAA Darwish, SE Al Garni, HI ElSaeedy, KF Abd El-Rahman et al. (2016) Influence of thickness and annealing

on linear and nonlinear optical properties of manganese (III) chloride tetraphenyl porphine (MnTPPCl) organic thin films. Infrared Physics & Technology, 78: 77–83.

27. Amr Attia Abuelwafa, MS Abd El-sadek, Sahar Elnobi, Tetsuo Soga (2021) Effect of transparent conducting substrates on the structure and optical properties of tin (II) oxide (SnO) thin films: Comparative study. Ceramics International. 47(10) Part A, 2021: 13510-8.

28. MM Shehata, H Kamal, HM Hasheme, MM El-Nahass, K Abdelhady (2018) Optical spectroscopy characterization of zinc tetra pyridel porphine (ZnTPyP) organic thin films. Optics & Laser Technology, 106: 136-44.

29. H Ticha, L Tichy (2002) Semiempirical relation between non linear susceptibility (refractive index), linear refractive index and optical gap and its application to amorphous chalcogenides, J. Optoelectron. Adv. Mater, 4: 381-6.

30. Rashmi Chauhan, Amit Kumar Srivastava, Arvind Tripathi, Krishna Kant Srivastava (2011) Linear and nonlinear optical changes in amorphous As2Se3 thin lm upon UV exposure, Prog. Nat. Sci.: Mater. Int, 21: 205–10.

31. Ladislav Tichý, Helena Tichá, Karel Handlír (1987) Chalcogenide and other glasses Photoinduced changes of optical properties of amorphous chalcogenide films at ambient air pressure. Journal of Non-Crystalline Solids 97–98, Part 2, 2 1987: 1227-30.

32. B Shanmugavelu, VVRK Kumar, R Kuladeep, DN Rao (2013) Third order nonlinear optical properties of bismuth zinc borate glasses. J. Appl. Phys, 114: 243103.

33. L Tsang, JA Kong, KH Ding (2004) Scattering of Electromagnetic Waves: Theories and Applications, Wiley, New York.

34. Q Shen, K Katayama, T Sawada, T Toyoda (2008) Characterization of electron transfer from CdSe quantum dots to nanostructured TiO2 electrode using a near-field heterodyne transient grating technique, Thin Solid Films, 516: 5927–30.

35. Savaş Sönmezoğlu, Özlem Ateş Sönmezoğlu (2011) Optical and dielectric properties of double helix DNA thin films, Mater. Sci. Eng. C, 31: 1619–24.